Level Set Methods for the Displacement of Layered Materials

J. A. Boon, C. J. Budd and G. W. Hunt
Centre for Nonlinear Mechanics, University of Bath, Bath BA2 7AY, UK

Previous multi-layered folding models have struggled to describe the geometry of the interfaces between layers. In the level set method a single function $\phi(x, y, t)$ can be used to encode all the information of a multi-layer material in which all layers are in contact and thus is a very natural way of dealing with the geometry. This paper shows the potential for the level set method (in multi-layer problems) by demonstrating that it can describe the geometry of multi-layer folding patterns including those with singularities. The method is then applied to describe the mechanics of the modelling of parallel folding in multi-layered structures.

Keywords: Level Set Method, parallel folding, layered material, energy methods

1. Introduction

Deformation patterns of multi-layered materials under compression are strongly influenced by the way that the layers interact and slide over each other, and hence are quite different from the folding patterns of homogeneous materials. Such folding arises naturally when layered materials are compressed in the plane of the layers, in a medium that allows them to slide over each other but not to separate. An important example occurs in the buckling of layered sedimentary rocks under tectonic compression. The same mechanisms also appear in the compression of layers of paper (for which we provide some experimental results), and in certain types of composite materials. Structural geologists have classified folds according to the geometry of their observed sections, and specific names have been given to those that frequently appear (Price & Cosgrove 1990). The geometry of these folds range from almost sinusoidal patterns, to the straight limbs and sharp corners of kink banding and chevron folding. However in all cases the resulting deformation is strongly influenced by the constraints of the multi-layered geometry – a subtle mix of *geometrical* constraints imposed by the need for the layers to fit together, and *mechanical* constraints of bending stiffness and interlayer friction.

Here we are mostly interested in *parallel folding* (folds where the orthogonal thickness remain constant). This occurs when a finite number of layers, loaded in their plane, deform into a softer surrounding medium (foundation or matrix) while slipping at their interfaces (Edmunds *et al.* 2006). Parallel folds formed under large overburden pressures would be expected to limit voids between the layers (carrying a large energy penalisation), and we therefore take the process to be one of buckling in the complete absence of voids (Budd *et al.* 2003; Edmunds *et al.* 2006)

Figure 1(a) shows an example of parallel folding in rocks with a layer thickness of around 10–25 cm. Since the layers fit together without voids, each has a slightly different geometry from its neighbour; as a consequence, a singularity can appear on one interface, as seen in the figure. Here the layers appear smooth (almost sinusoidal) at the bottom of the picture, but as we move towards the top they become increasingly constrained by the geometry, until at a particular interface

a singularity occurs. Past this singularity the layers take a non-differentiable 'V' shape which propagates without change as we move further up; this V shape is seen also in kink bands and in chevron folds (see figure 1(b)).

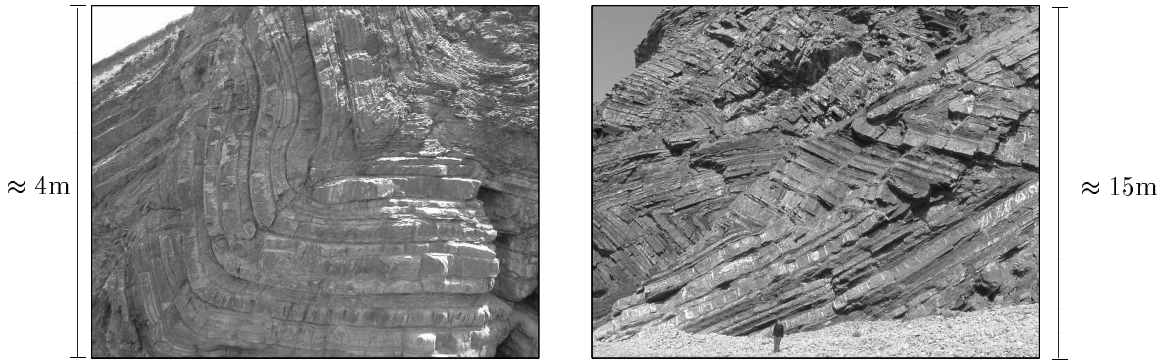

Figure 1. (a) Parallel folding of rocks near Bude, Cornwall. (b) Chevron folding of rocks at Millock Haven, Cornwall.

A series of experiments showing regular parallel folding in layers of paper has been undertaken by two of the current authors and figure 2 shows a typical outcome. Budd *et al.* (2003) presented a model for parallel folding in two flexible layers, subsequently extended to an n layer model in Edmunds *et al.* (2006). A method

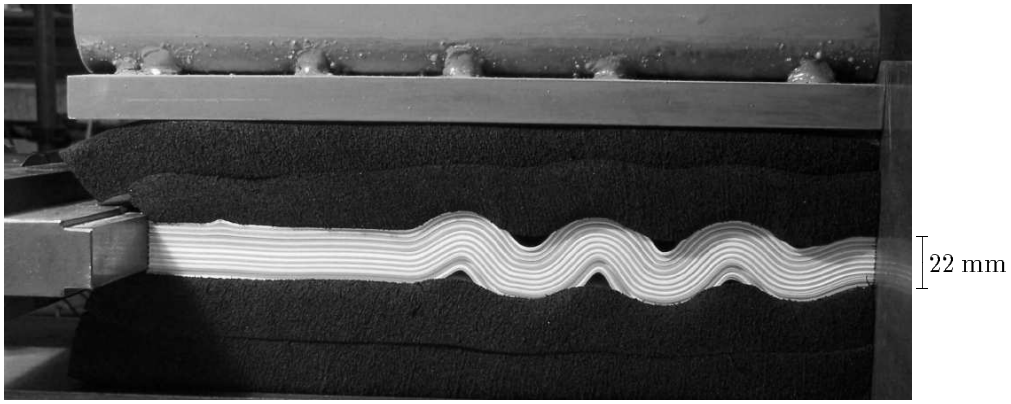

Figure 2. Parallel folding of 220 sheets of paper into foam. Here the black lines are for identification.

for modelling the fold geometry, proposed in Edmunds *et al.* (2006), considered a sinusoidal Galerkin approximation for the shape of the central layer, and simply extended it to the outerlayers. This technique is unable to deal with the geometrical constraints of multi-layer folding leading to singularities. This means that the associated problems of kink banding and chevron folding (layers bend with infinite curvature and straight limbs such that no voids form (figure 1(b))) require a separate treatment for what is essentially a similar problem (see for example Hunt *et al.* (2000); Wadee *et al.* (2004)).

Here we present a method for describing multi-layer parallel folding based on the level set approach. This naturally copes with the *geometry* of smooth parallel folding and also allows a consistent description of the geometry associated with singularity formation and kink banding (§2). The level set approach propagates the shape of the central layer at a prescribed rate in the normal direction. By doing this, the shapes of all outer layers can be determined (and controlled) rather than being just approximated. The normal propagation is achieved using the level set method (Dervieux & Thomasset (1979, 1981); Osher & Sethian 1988) in which a function $\phi(x, y, t)$ is introduced such that the shape of the layer indexed by t is given by the (x, y) curve satisfying $\phi(x, y, t) = 0$ (the zero level set). An application of this method to the rock layers pictured in figure 1(a) is shown in figure 3. A spline function has been fitted to a central layer (thick dashed line) and the resulting curve propagated in the normal direction by calculating ϕ. We see that all of the important geometrical features of the layers are resolved, including the cusp and singularity formation as we propagate in the upwards direction and the simple geometry in the downwards direction. To apply this method to find the actual form of a deformed material requires information only about the shape of a single reference layer. The level set method then gives the position of all the other layers and encodes all of the information of the geometry in terms of ϕ. Additional information about the *mechanical* behaviour of the system, in particular the bending energy, the work done by friction and the work done in compressing the embedding medium is then determined for the individual layers. This provides a total potential energy function for the whole system of the deformed layers, which when coupled to the geometrical description of the layers given by the level set method contains a significant (stiffening) nonlinearity. We then look for states which are stationary points of this energy functional. As the energy can be expressed in terms of the single function ϕ this calculation becomes relatively straightforward.

The paper first describes the geometry of multi-layer folding, showing that it naturally leads to the formation of singularities. We then describe the level set method for calculating this geometry, and will discuss its performance and errors when singularities are present. Following this we make use of the level set method to construct a potential energy function for the deformed material. Here we will only look at such an energy functional up to a singularity which we take as the limit of the folding pattern. (Beyond this, elasticity assumptions would be expected to break down.) From this energy functional we deduce the profile of the deformed multi-layer material.

2. The geometry of multilayer folding

We now consider the basic process involved in the folding of multi-layer materials, using first a Lagrangian approach to describe the geometry of the patterns that can be observed. A natural consequence of this is the demonstration that singular behaviour arises very naturally in the folding of such materials.

(*a*) *The basic folding processs*

Sedimentary rocks can be formed under the sea bed as loose particles (sediments), layed down layer upon layer, and forced together by the overburden pres-

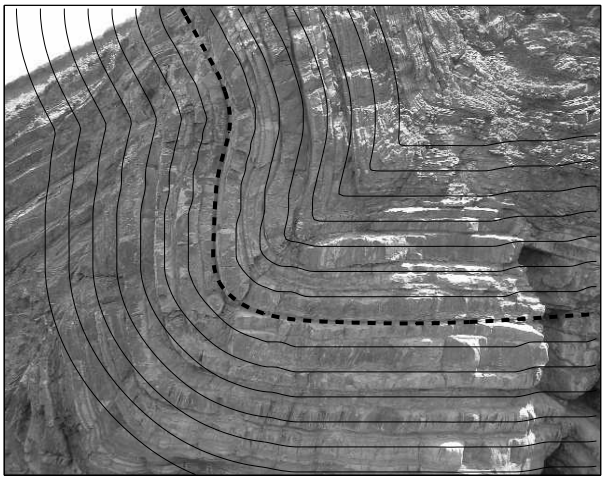

Figure 3. The Level Set Method applied to folding rock. The thick dashed line is a spline fitted to the shape of the rock layer

sure, caused by the material above. This process forms horizontal layers, which fold when tectonic plate movement produces an axial load (figure 4). In this figure we see identical layers of length L and width Δt, under an overburden pressure q, undergoing an end-shortening due to the compressive load.

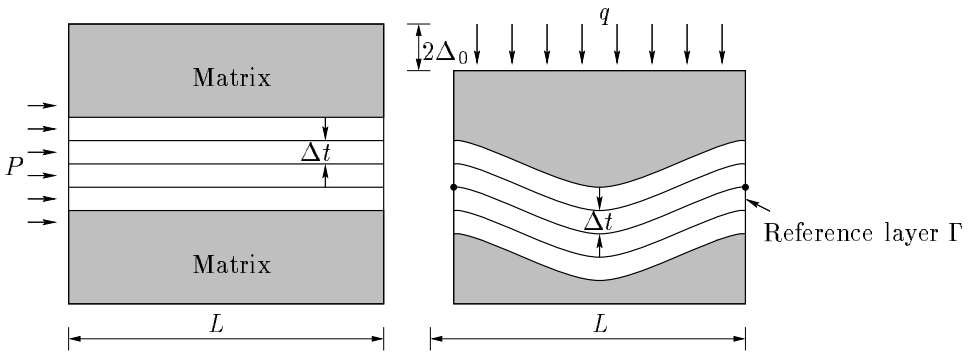

Figure 4. The assumed geometry showing the compressive force P and the overburden pressure q. Note that the angle of the layers with the horizontal at the endpoints is assumed to be zero.

Consider a layered material to be characterized by the position of each layer. We can then consider curves Γ_t, indexed by t, which describe the interface between layers. To describe such a layered material let the upper surface of top layer be described by the curve $\Gamma_{n\Delta t}$ and the lower surface of the bottom layer by the curve $\Gamma_{-n\Delta t}$ with the interfaces between the other layers described by the curves $\Gamma_{i\Delta t}, -n < i < n$. In *parallel folding* we consider a situation where the layers are always in contact and for which the curves $\Gamma_{i\Delta t}$ are separated by a *constant* normal distance Δt. The geometry of a set of curves with parallel folding can then be described by taking a *reference curve* (without loss of generality Γ_0) and propagating this curve in a normal direction a distance $i\Delta t$ to give the curve $\Gamma_{i\Delta t}$. Generally,

the shape of Γ_i will differ from Γ_0 (although the chevron folding phenomenon of figure 1(b) gives an example where an identical family of curves can coexist). In particular, an initially smooth curve Γ_0 may give rise to curves $\Gamma_{i\Delta t}$ with singularities and sharp corners, as seen in figure 1. To propagate past such a singularity great care needs to be taken.

(*b*) *The Lagrangian representation of parallel folding*

We now give a Lagrangian calculation of the process of parallel folding and show that the length of the interface is conserved, provided: a) the surface remains smooth (ie. no singularities develop); and b) the angle of the interface with the horizontal is the same at either end. To describe the folding process we consider the set of curves given parametrically by $\Gamma_t : R^2 \rightarrow R^2$ so that $\Gamma_t = \{(x(s,t), y(s,t)) : s \in [0,1]\}$. The parallel folding assumption is that the *normal separation* between two curves parametrized by $t = t_1$ and $t = t_2$ is given by $|t_2 - t_1|$ and does not depend on s. This assumption leads to a simple construction of the *entire* set of curves for all t, given a reference curve for $t = 0$. The exact position of Γ_i at time t may be constructed by advancing each point of Γ_0 in its unit normal direction, $\mathbf{n}$, a distance $t = i\Delta t$ (Sethian 1999) (figure 5) where

$$\mathbf{n} = \frac{(-y_s^0, x_s^0)}{\sqrt{(x_s^0)^2 + (y_s^0)^2}}. \tag{2.1}$$

Here the suffix 0 refers to the reference curve.

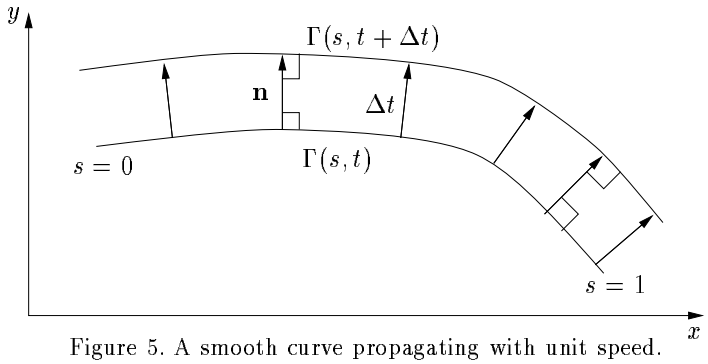

Figure 5. A smooth curve propagating with unit speed.

It follows from standard analysis that for each fixed $t = i\Delta t$ the Lagrangian description of Γ_t takes the form

$$\Gamma_t = \{(x(s,t), y(s,t)) = \left(\frac{-y_s^0 t}{((x_s^0)^2 + (y_s^0)^2)^{\frac{1}{2}}} + x^0(s), \frac{x_s^0 t}{((x_s^0)^2 + (y_s^0)^2)^{\frac{1}{2}}} + y^0(s) \right)\} \tag{2.2}$$

Equation (2.2) is valid for all $t = i\Delta t$, although the resulting curve may have points of singularity characterized by a lack of a well-defined normal vector. To find $x_s(s,t)$ and $y_s(s,t)$ we differentiate equation (2.2) with respect to s to obtain:

$$x_s(s,t) = \frac{-((x_s^0)^2 + (y_s^0)^2)^{\frac{1}{2}} y_{ss}^0 t + y_s^0 t(\frac{1}{2}((x_s^0)^2 + (y_s^0)^2)^{-\frac{1}{2}}(2x_s^0 x_{ss}^0 + 2y_s^0 y_{ss}^0))}{(x_s^0)^2 + (y_s^0)^2} + x_s^0 \tag{2.3}$$

and

$$y_s(s,t) = \frac{((x_s^0)^2 + (y_s^0)^2)^{\frac{1}{2}} x_{ss}^0 t - x_s^0 t(\frac{1}{2}((x_s^0)^2 + (y_s^0)^2)^{-\frac{1}{2}}(2x_s^0 x_{ss}^0 + 2y_s^0 y_{ss}^0))}{(x_s^0)^2 + (y_s^0)^2} + y_s^0. \tag{2.4}$$

These expressions can be simplified by considering the curvature κ

$$\kappa(s,t) = \frac{y_{ss}x_s - x_{ss}y_s}{(x_s^2 + y_s^2)^{\frac{3}{2}}} \quad \text{so that} \quad (x_s(s,t), y_s(s,t)) = (x_s^0, y_s^0)(1 - \kappa(s,0)t). \tag{2.5}$$

We make the significant observation that this vector vanishes (and hence we can not define a normal vector) when $t = 1/\kappa(s,0)$ which is the radius of curvature of the reference curve at this point. By moving forward t and then backwards by the same amount, it is immediately clear that $(1 - \kappa(s,0)t)(1 + \kappa(s,t)t) = 1$ so that

$$\kappa(s,t) = \frac{\kappa(s,0)}{1 - \kappa(s,0)t} \tag{2.6}$$

Note that the curvature $\kappa(s,t)$ becomes infinite at the first value of t which occurs on the normal through the point on the reference curve with the *smallest radius of curvature*. If $\kappa(0,s)$ is *negative* then the curve Γ_t has a well defined normal for all positive t. However, if $\kappa(s,0)$ is *positive*, then there will be a first value of $t = T = \min(1/\kappa(s,0))$, at which the normal vector first vanishes. The value of T gives the maximum width of the layers before a singularity occurs. For $t > T$ the curve Γ_t is multi-valued and has a swallow-tail singularity, with points of infinite curvature. This situation is illustrated in figure 6 where we take a parabola to be the reference curve.

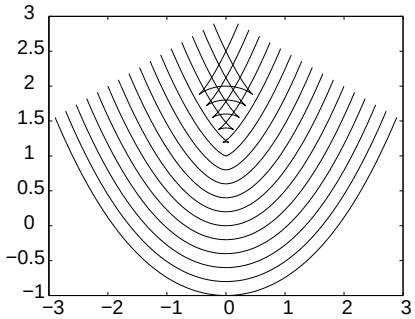

Figure 6. Propagation of a parabolic reference curve Γ_0 showing the formation of the swallow-tail singularity

As the layers are assumed to be incompressible in their local tangent direction, it follows that the *arc-length* of each layer must remain constant. This imposes a

constraint on the allowable deformations. To consider the effects of this constraint we calculate the arc-length. Suppose that $d\sigma_t$ is the infinitessimal arc-length on the curve Γ_t. If the total arc-length of Γ_t is σ_t, then

$$\sigma_t = \int_{\Gamma_t} d\sigma_t = \int_{\Gamma_t} \frac{d\sigma_t}{ds} ds.$$

Now

$$\frac{d\sigma_t}{ds} = \sqrt{x_s^2(s,t) + y_s^2(s,t)} = \sqrt{(1-\kappa_{s,0}t)^2}\frac{d\sigma_0}{ds} = |1-\kappa_{s,0}t|\frac{d\sigma_0}{ds}.$$

Two cases then arise: either $t < T$ in which case $1 - \kappa_{0,s}t$ has a constant sign over the length of Γ_t; or it changes sign at certain points along the curve. If $\theta(s,t)$ is the angle of the curve Γ_t at the point. $(x(s,t), y(s,t))$, then $\tan(\theta) = dy/dx$ and $\kappa = \partial\theta/\partial\sigma$. Thus, if $t < T$ we have

$$\sigma_t = \int_{\Gamma_t} \frac{d\sigma_t}{ds} ds = \int_{\Gamma_0} (1 - t\kappa(s)) \frac{d\sigma_0}{ds} ds = \sigma_0 - t\int_{\Gamma_0} \frac{d\theta_0}{ds} ds = \sigma_0 - t\left[\theta(s,0)\right]_{s=0}^{s=1}.$$

We arrive at the result:

Theorem 2.1. *Whilst equation* (2.2) *holds and* $t < T$ *total arc-length of* Γ_t *is given by:*

$$\sigma_t = \sigma_0 - t[\theta(s,0)]_{s=0}^{s=1} \tag{2.7}$$

Corollary 2.2. *If* $t < T$ *and* $[\theta(s,0)]_{s=0}^{s=1} = 0$, *the total arc-length of each curve* Γ_t *remains constant.*

If $t > T$ then the normal ceases to exist, and the direction of $d\sigma/ds(t)$ changes sign at certain points so that $|1 - t\kappa(s,0)|$ changes from $1 - t\kappa(s,0)$ to $-1 + t\kappa(s,0)$. The above reasoning breaks down, and there is no guarantee that the total arc-length is preserved.

(c) *Singularities*

If $t > T$ the curve Γ_t has a singularity resulting in a self-intersecting curve with infinite curvature. We now explore what happens $t \to T^-$. To study this situation we consider what happens when a parabola is propagated forward at a constant speed. We take a reference curve Γ_0 defined for $s \in [0,1]$ by

$$x(s,0) = s - 1/2, \quad \text{and} \quad y(s,0) = \frac{K(s-1/2)^2}{2}.$$

If we set $S = (s - 1/2)$ then the unit normal $\mathbf{n}$ is given by

$$\mathbf{n} = \left(-\frac{KS}{\sqrt{1+K^2S^2}}, \frac{1}{\sqrt{1+K^2S^2}}\right)$$

and hence

$$(x(S,t), y(S,t)) = \left(S - \frac{KSt}{\sqrt{1+K^2S^2}}, \frac{KS^2}{2} + \frac{t}{\sqrt{1+K^2S^2}}\right).$$

A plot of the resulting set of curves was given in figure 6 where the self-intersecting nature of the curve is clear. The radius of curvature of the reference curve Γ_0 takes its smallest value of $1/K$ when $S = 0$ and we deduce that the singularity occurs when $t = T = 1/K$. If $t > 1/K$ then the curve self-intersects when $(x(S,t), y(S,t)) = (x(-S,t), y(-S,t)) = (0, Y)$ which occurs when

$$S = \sqrt{t^2 - 1/K^2} \quad \text{and} \quad Y = Kt^2/2 + 1/2K.$$

At the point of self-intersection the curve Γ_t has a locally V-shaped form. The gradient of the curve is given by $dy/dx = y_s/x_s$. Substituting $K^2S^2 = 1 + K^2t^2$ into the expressions for y_s and x_s we have that at the point of self-intersection

$$dy/dx = \pm K\sqrt{t^2 - 1/K^2}, \quad \text{if} \quad t > 1/K. \tag{2.8}$$

To examine the form of the curves as we approach the singular point we set $t = 1/K - \delta$ and let S and $\delta > 0$ be small. To leading order we then have

$$x = \delta KS + \frac{K^2S^3}{2} + \mathcal{O}(S^5, \delta S^3) \quad \text{and} \quad y = \frac{1}{K} - \delta + \frac{\delta K^2 S^2}{2} + \frac{3K^3}{8}S^4 + \mathcal{O}(S^6, \delta S^4).$$

It follows that

$$y = \frac{1}{K} + \frac{3K^{1/3}}{8}(2x)^{4/3} + \mathcal{O}(x^2) \quad \text{if} \quad \delta = 0, \quad y = 1 - \frac{x^2}{2\delta} + \mathcal{O}(x^4) \quad \text{if} \quad 0 < \delta \ll 1.$$

It follows immediately that when $x = 0$ we have $d^2y/dx^2 = \infty$ if $\delta = 0$ and $d^2y/dx^2 = K/\delta$ if $0 < \delta \ll 1$. This calculation is significant in the context of the calculation of the mechanics of buckling that we will consider in §4. In particular, the bending energy associated with a buckled layer is proportional to the integral of the square of the second derivative which, we show in §4 approaches infinity as $\delta \to 0$. As a consequence, the buckling energy is a strongly nonlinear function of the displacement of the reference layer, and this has a significant effect on the resulting buckling profiles.

It is difficult to know exactly what happens to the rock layers physically as a singularity is approached and possibly transgressed. However, the assumed geometry forces this to happen and a comparison of figure 1 and figure 6 shows clear similarities. What is clear, however, is that the rocks do not pass through themselves. Indeed, what seems to occur is that the rock layers of figure 3 (shown as a dashed line) take the geometry of the *non self-intersecting* part of the curve. Hence, to fully realise the possible geometries that a rock layer can have, we are motivated to look at a construction method which is different from the Lagrangian approach (which leads to the self-intersecting curves) and which allows us naturally to resolve, and pass through, the singularity, allowing a natural description of the non self-intersecting part of the curves when $t > 1$ where appropriate. Such a procedure is given by the level set method, which relies on an Eulerian representation of the set of layered surfaces and a weak formulation of the equation of propagation of the layers. Sethian (1985) uses an *entropy condition* to overcome the problems with self-intersection that arise in the Lagrangian framework. Informally, this strategy evolves the front according to (2.2) until there is a collision in the normals. The curves that collide are then eliminated and the front is moved continuously along

the remaining normal curves, all along removing those that collide. It is this process of deleting the swallow-tail that causes the loss in length. This process is equivalent to using a numerical method to solve the level set equation described in the next section to give a regularized (viscosity) solution.

3. The Eulerian representation, the theory of level sets and the viscosity solution

(*a*) *The Eulerian representation and the level set method*

In contrast to the previous description of layer propagation using Lagrangian coordinates, the Eulerian representation aims to find the (x, y) equation of the curves Γ_i thinking of t as a continuous variable and looking at the differential equations governing the propagation of Γ as a function of t. Accordingly, for a general t we set $\Gamma_t = \{(x, y) : y = w(x, t)\}$. We suppose further that each set Γ_t occupies a part of a bounded, rectangular domain Ω in $\mathbb{R}^2$ extending from the left boundary of Ω to the right and separating Ω into two regions, Ω^-, the region *'inside'* the boundary and Ω^+, the region *'outside'* the boundary. We next assume that Γ_t is a *level set* of a higher dimensional function $\phi(x, y, t)$ so that

$$y = w(x, t) \quad \text{iff} \quad \phi(x, y, t) = 0.$$

The evolution of the function ϕ with t can then be linked to the propagation of the interfaces Γ_t. This is the essence of the level set method (LSM). References to the the level set method, and in particular its application to the calculation of various free surface problems in fluid mechanics, include Osher & Sethian (1988), Osher & Fedkiw (2003) and Sethian (1999). To apply the level set method, we first find

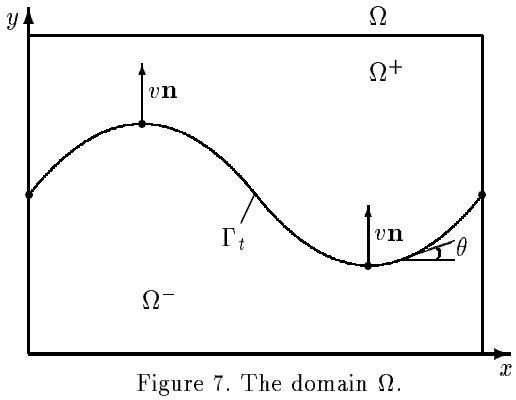

Figure 7. The domain Ω.

ϕ by solving an appropriate partial differential equation, and then determine its contours. As an example of the use of the LSM, consider the function

$$\phi(x, y, t) = x^2 + y^2 - (1 + t)^2$$

then for fixed t the (x, y) curve satisfying the level set equation $\Gamma_t = \{(x, y) : \phi(x, y, t) = 0\}$ is a circle of radius $(1 + t)$. The family of such level sets precisely describes the evolution of an initial circle propagating at a constant speed $v = 1$ in

a direction normal to each curve. Figure 8 shows how the function ϕ above evolves with t.

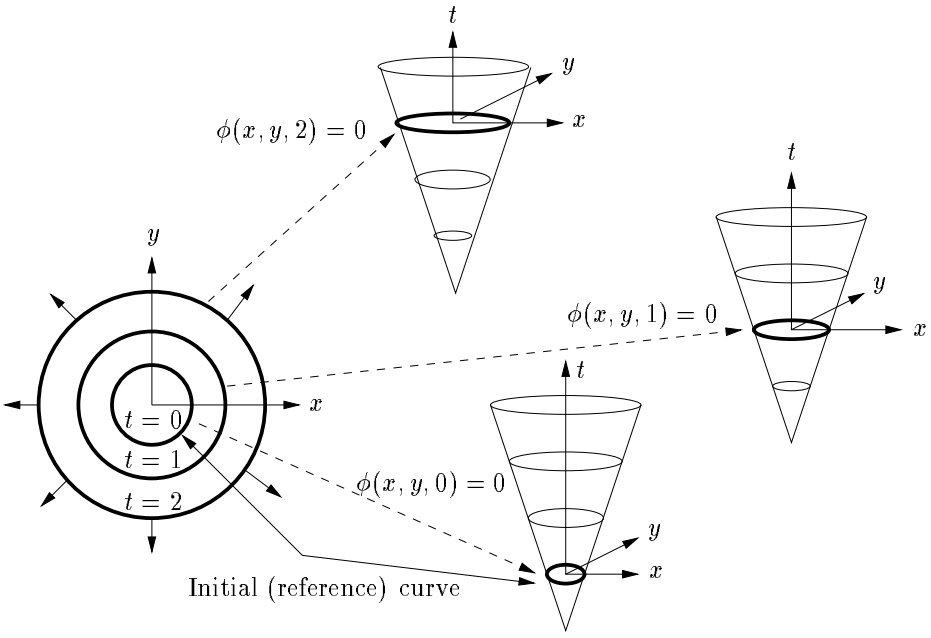

Figure 8. The propagation of a circle in the normal direction by considering a higher dimensional function $\phi(x, y, t)$. (After Sethian (1999))

We now return to the general case and derive the partial differential equation satisfied by the function $\phi(x, y, t)$. Following the formulation of Sethian (1999), let $\mathbf{x}(t) = (x(t), y(t))$ be a point on the curve $\Gamma_t \equiv \{(x, y) : y = w(x, t)\}$. Starting from the identity $\phi(x, y, t) = 0$, it follows from the chain rule that,

$$\phi_t + \nabla\phi(\mathbf{x}(t), t) \cdot \mathbf{x}'(t) = 0, \tag{3.1}$$

where $\nabla\phi$ is defined to be (ϕ_x, ϕ_y). If $\mathbf{v}(x, y)$ is the speed in the normal direction, then $\mathbf{x}'(t) \cdot \mathbf{n} = v$, where the unit normal $\mathbf{n}$ is given by $\mathbf{n} = \nabla\phi/|\nabla\phi|$. It follows that ϕ satisfies the following hyperbolic partial differential equation of Hamilton–Jacobi type (the *level set equation*).

$$\phi_t + \mathbf{v}.|\nabla\phi| = 0. \tag{3.2}$$

Solving this equation for $\phi(x, y, t)$ together with a prescribed initial function $\phi(x, y, 0)$ determines the curves $\Gamma_t = \{(x, y) \mid \phi(x, y, t) = 0\}$ and the exterior and interior regions:

$$\Omega_t^+ = \{(x, y) \mid \phi(x, y, t) > 0\} \quad \Omega_t^- = \{(x, y) \mid \phi(x, y, t) < 0\} \tag{3.3}$$

In the level set formulation, the condition for *parallel folding* is that the speed function, $\mathbf{v}(x, y)$ should be *constant*. However, we note that it would be straightforward to include other forms for the function $\mathbf{v}$ to allow, for example, for situations in which the rocks can compress laterally (Wadee *et al.* 2004). Other examples of speed

functions include the cases where $\mathbf{v}$ depends on the curvature κ (which arises in flame front propagation (Rhee *et al.* 1995)) and where it depends on $|\nabla\phi|$ (which arises in electro-machining). With this formulation the important properties (see figure 4) of the geometry of the layers of rock can be easily calculated in terms of ϕ.

(*b*) *Numerical implementation*

To propagate the interface using the level set method we calculate the whole function ϕ using a time-stepping method. Assuming that we have a good approximation to $\phi(x, y, t)$ for some time $t = i\Delta t$ we first use a numerical method to find an approximation to the solution ϕ of (3.2) for the time level $t = (i + 1)\Delta t$. A second numerical method is then used to locate the zero contour of $\phi(x, y, (i+1)\Delta t)$ to find an approximation to $\Gamma_{(i+1)\Delta t}$. The algorithm we use for implementing this strategy is as described in Osher & Sethian (1988). To implement this we consider an approximation $\Phi^n_{j,k}$ to the function $\phi(x, y, t)$ at the point $(x, y, t) = (jh, kh, n\Delta t)$. Here h and Δt are small and constant. An explicit discretisation of (3.2) for a constant $\mathbf{v}$ takes the form

$$\Phi^{n+1}_{k,j} = \Phi^n_{k,j} - \Delta t \left[\max(v, 0)\nabla^+ + \min(v, 0)\nabla^-\right] \tag{3.4}$$

where

$$\begin{aligned} \nabla^+ \quad = \quad & [\max(D^{-x}_{k,j}, 0)^2 + \min(D^{+x}_{k,j}, 0)^2 + \\ & \max(D^{-y}_{k,j}, 0)^2 + \min(D^{+y}_{k,j}, 0)^2]^{1/2} \end{aligned} \tag{3.5}$$

$$\begin{aligned} \nabla^- \quad = \quad & [\max(D^{+x}_{k,j}, 0)^2 + \min(D^{-x}_{k,j}, 0)^2 + \\ & \max(D^{+y}_{k,j}, 0)^2 + \min(D^{-y}_{k,j}, 0)^2]^{1/2}. \end{aligned} \tag{3.6}$$

In the above the terms $D^{+x}_{j,k}$ etc. are a shorthand for the difference operators defined by

$$D^{+x}_{j,k} = \frac{\Phi^n_{j+1,k} - \Phi^n_{j,k}}{h}, \quad D^{-x}_{j,k} = \frac{\Phi^n_{j,k} - \Phi^n_{j-1,k}}{h}, \tag{3.7}$$

with similar expressions for $D^{+y}_{j,k}, D^{-y}_{j,k}$. Local errors in this scheme are of $\mathcal{O}(h, \Delta t)$. The level set method as implemented is stable provided that the Courant–Friedrichs–Lewy condition (Courant *et al.* 1928) is met. There are three sources of error when numerically solving the level set equation (Sethian 1999). These are the *Initialization error* which is error obtained when finding the signed distance function on a discrete mesh from an initial curve, the *Update error* which is error in finding an approximation to $\phi(x, y, n + 1\Delta t)$ given $\phi(x, y, n\Delta t)$ and the *Measurement error* which is the error associated with the finding the position of the zero level set using, for example, the MATLAB `contour` routine. Note that in order to calculate Φ^{n+1} we must calculate Φ^n at *all* spatial points, not just those close to the interface. This is an inefficiency in the method. We note that there are more efficient schemes such as the 'Narrow Band Method' (Chopp 1993), in which the only entries to be updated are those in a narrow band around the interface. Once the interface reaches

the edge of the band the signed distance function is re-calculated, the narrow band is re-formed around the current position of the interface and the problem is solved until the interface hits the edge of the band again and so on. Hence, a balance is struck between saving time for updating only a small number of elements and the cost of re-calculating the signed distance function.

(*c*) *Convergence of the LSM and the viscosity solutions*

The level set equation (3.2) considered in the current paper is an example of a wider class of equations called *Hamilton–Jacobi* equations, given by

$$\phi_t + H(\nabla\phi, \phi) = 0 \qquad \text{for } x \in \mathbb{R}^m \times (0, \infty) \tag{3.8}$$

The function H is the *Hamiltonian* which for our purposes is given by

$$H(\phi_x, \phi_y) = v\sqrt{\phi_x^2 + \phi_y^2} \tag{3.9}$$

In general there can be no smooth solution to equation (3.8) lasting for all times $t > 0$. This corresponds precisely to the swallow-tail singularity observed in the previous section. However, we may regularize the Hamilton–Jacobi equation by adding artificial viscosity, $\epsilon\Delta\phi^\epsilon$, with $\epsilon > 0$ to give

$$\phi_t^\epsilon + H(\nabla\phi^\epsilon, \phi^\epsilon) - \epsilon\Delta\phi^\epsilon = 0 \qquad \text{for } x \in \mathbb{R}^m \times (0, \infty) \tag{3.10}$$

In general, provided $\epsilon > 0$, equation (3.10) admits smooth solutions. If the solutions ϕ^ϵ of (3.10) converge weakly to a function ϕ as $\epsilon \to 0$, then this is a weak solution of (3.8). It is called the *viscosity solution* and can have gradient discontinuities (Crandall & Lions 1983; Crandall *et al.* 1984).
The viscosity solution picks out the correct weak solution when no classical solution exists. Informally, the viscosity solution 'deletes' the multivalued part of the swallow-tail curve. In the numerical implementation of the level set method, that we have presented, the regularisation is automatically provided by the numerical truncation error which introduces an artificial viscosity term. The numerical method is effectively solving a problem close to (3.10) with $\epsilon \approx \mathcal{O}(h)$ (Enright & Fedkiw 2003). Consequently, the numerical method will give solutions close to the viscosity solution, thus automatically smoothing out the singularities and regularizing the sharp corners.

(*d*) *Singularities found in rock folding*

We conclude this section by looking at some examples in which we explore the applications and limitations of the LSM for calculating the geometry of certain problems given a known reference layer Γ_0.

(i) *Examples with reentrant corners*

Example 1 As a first, quantitative calculation, which has a close link to a rock folding problem which we will consider further in §4, we consider a reference curve given by $\Gamma_0 = \{(x, y) : x = s, y = \cos(2\pi s)\}, \quad 0 \le s \le 1$. To apply the LSM we take an initial function $\phi(x, y, 0) = y - \cos(2\pi x)$. This is not a *signed distance*

function, meaning that gradients are steeper and therefore harder to approximate accurately numerically, but it does give an accurate and easy to implement initial zero level set. We now compute the resulting layers Γ_t and compare these with the solutions predicted by the Lagrangian formulation. Using this, the exact parametric equation of the layer at the time t is given by

$$x = s + \frac{2\pi \sin(2\pi s)t}{\sqrt{1 + 4\pi^2 \sin^2(2\pi s)}}, \quad y = \cos(2\pi s) + \frac{t}{\sqrt{1 + 4\pi^2 \sin^2(2\pi s)}}.$$

The curvature of the reference curve takes its maximum value of $4\pi^2$ at the point $s = 1/2$ and hence a singularity occurs when $t = 1/4\pi^2$, $x = 1/2$, $y = -1 + 1/4\pi^2$. A close-up of the singularity of the exact (multi-valued) solution arising from the Lagrangian description is plotted in figure 9(a).

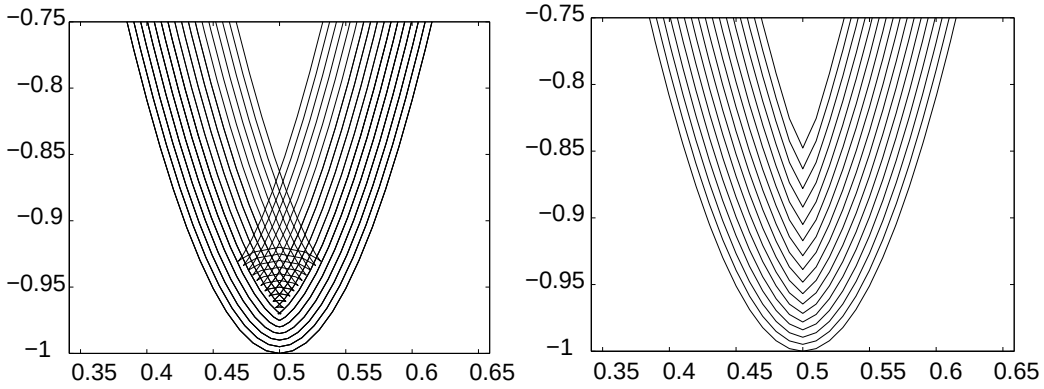

Figure 9. Close-up of a propagation of a cosine wave (a) using the Lagrangian method, showing the self-intersecting curves. (b) using the LSM, showing the local V-shaped nature of the curves.

We now compare the Lagrangian solution with that derived by using the LSM. A calculation using the method for $h = 0.01$ and $\Delta t = 0.005$ is presented in figure 9(b) (here the corresponding close-up of the singularity is shown). Observe, that in contrast to the Lagrangian description, the LSM has deleted the self-intersecting part of the curves, and the resulting curves have an apparent gradient discontinuity at the centre. The local V-shaped nature of these curves is very similar to that of the layers in the chevron folding pattern illustrated in figure 1(b). Indeed, if we take Γ_0 to be the V-shaped curve $\Gamma_0 = \{(x, y) : x = s, y = |s - 1/2|\}$, then the resulting calculation of the layers Γ_t using the LSM is given in figure 10(a) and a close-up in figure 10(b). We see that the LSM has succesfully coped with the gradient singularity, reproducing the self-replicating feature of parallel folding in this case where all layers Γ_t have the exactly the same shape and the same arc-length. We note that in figure 10(b) the corner is slightly smoothed due to the error. This effect can be reduced by refining the mesh.

As a further measure of the accuracy of the calculation of the propagating cosine reference curve $\Gamma_0 = \{(x, y) : x = s, y = \cos(2\pi s)\} \quad 0 \leq s \leq 1$, we plot the total arc-length of the resulting curves. The choice of reference curve ensures that $[\theta_t] = 0$. Hence, from theorem 2.1, the total arc-length of the curve Γ_t stays constant up to

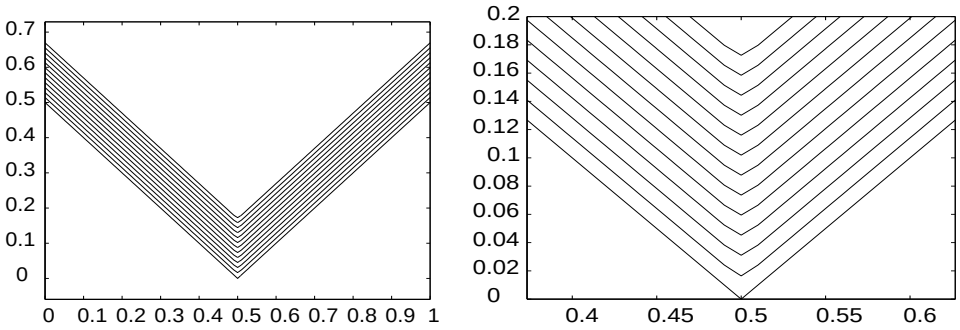

Figure 10. (a) Propagation of a V-shaped curve with the LSM (b) Close-up of the singularity showing the local error

the point of singularity formation when $t = 1/4\pi^2$. For larger values of t the curve self-intersects and the total arc-length of the curve omitting the self-intersecting part decreases until a steady state is reached. This arc-length can be calculated exactly. If $s = s^*$ is the parameter value on the reference curve for which the normal intersects with the line $x = 1/2$ then

$$t = \frac{(1/2 - s^*)\sqrt{1 + 4\pi^2 \sin^2(2\pi s^*)}}{2\pi \sin(2\pi s*)}.$$

As the normal to the reference curve is also normal to Γ_t the angle θ is given by $\theta = -2\pi \sin 2\pi s$. The arc-length $\sigma(t)$ is then given by theorem 2.1 as

$$\sigma(t) = 2\int_{s^*}^{1} \sqrt{1 + 4\pi^2 \sin^2(2\pi s)}\, \mathrm{d}s + 2t\theta \tag{3.11}$$

This is a standard elliptic integral and can be evaluated analytically. Similarly the arc-length of Γ_t can be found numerically by applying quadrature to the sets found by the LSM. The two values are compared in figure 11.

Example 2. As a second example of an application of the LSM method we consider again the calculation illustrated in figure 3. A reference layer Γ_0 was obtained directly from the photograph by sampling the photographed curve at regular points at a roughly middle layer and then fitting a spline through the resulting data. The resulting layers propagated (through the singularity) by solving the level set equation (3.2). Here we took $h \approx 5$ and $\Delta t \approx 2.5$, and chose to plot the zero level set at every 15 time steps (there are 640 pixels in the horizontal direction). The qualitative agreement between the calculations and the observed geometry appears very good, including apparently the representation of the singularity and of the rock layers formed beyond the singularity.

(ii) *Examples with salient corners*

The viscosity solution does not always agree with the observed patterns of folded rock. In the photograph of figure 1(b) we see an example of *chevron folding* in which rock layers fold in a zig-zag with both reentrant and salient corners, each of which has a gradient discontinuity. Now consider a reference curve Γ_0 given by an upside-down 'V' with interior angle 2α and propogate this in the direction of incresing t

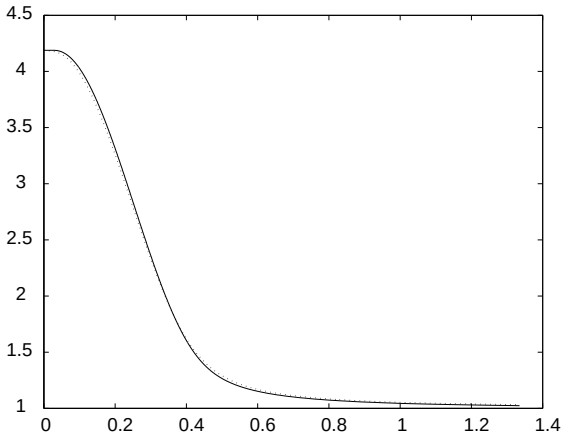

Figure 11. Change in arc length with t showing the LSM estimate (dotted) and the quadrature estimate (solid)

(see figure 12). Instead of propagating such a salient corner without change, the artificial viscosity in the LSM picks out a rarefaction fan of solutions in which the curves Γ_t lose the sharp V-shape and have a circular arc at the peak with arc-length $2t\alpha$. The LSM has not in this case given a solution consistent with that observed in practice. To overcome this difficulty we could follow the procedure outlined in Russo & Smereka (2000) in which the level set method is used to describe crystal growth with sharp corners. In such a method additional slip is introduced between the layers. This has the advantage of preserving the total arc-length of the solution, but we shall not consider this approach in the present paper.

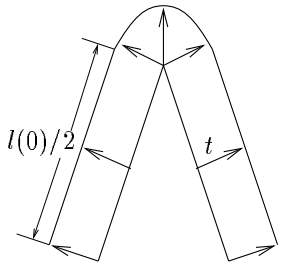

Figure 12. A Salient Corner obeys Huygens' Principle, forming a Rarefaction fan.

4. The mechanics of folding

Having determined a procedure for finding the overall geometry of the layered system from a single reference layer Γ_0 we now examine how the form of Γ_0 itself can be calculated by using properties of the function ϕ. This section shows how we can incorporate mechanical features into the geometrical description given by the level set method, allowing us to find the shape of the reference curve. The profile of the compressed layered material is determined by the interplay of several mechanisms namely the effect of the applied force, the bending properties of the layers, the work done into the external medium, the effects of the geometry constraints and

the frictional forces acting to oppose sliding between the layers. These are best described by calculating the total energy V which is a combination of the bending energy, frictional energy and the work done by the external forces. Crucially, this total energy, V can be calculated in terms of the level set function ϕ, depending on Γ_0. We can then find the profile of the material by finding stationary points of V with respect to (appropriate) variations in Γ_0.

(*a*) *Total energy in terms of* ϕ

We consider the geometry illustrated in figure 4 in which we assume that an initially undeformed multi-layer material enclosed within a foundation material is compressed and buckled by an external load. This load is resisted by the stiffness of the layers, the frictional force as the layers slide in contact and the resistance of the matrix in which the layers are embedded. In Budd *et al.* (2003) the potential energy of two axially and transversely incompressible layers of small thickness t in contact along an interface line was considered. In this the two layers each comprised a material of bending stiffness EI, which was embedded in a soft foundation of transverse stiffness k per unit length, and compressed longitudinally by a horizontal distance $\mathcal{E}$ (the *end-shortening*) by a load P. In Budd *et al.* (2003) the total energy was decomposed into four components: V = Bending Energy + Foundation Energy − Work Done by Load + Work Done against Friction, or

$$V = U_B + U_F - P\mathcal{E} + \chi U_\mu \tag{4.1}$$

The function $\chi = \pm 1$ is included in (4.1) as a *friction indicator* which ensures that the friction makes a positive contribution to the total potential energy when friction opposes the external force, and conversely, makes a negative contribution when friction acts in the same sense as the external force. For details on the interaction between χ and μ see Budd *et al.* (2003). In this two layer model we let w be the vertical deflection of the interface between the layers, x the horizontal distance and σ the arc-length. The total length of each of the layers is a constant L. Expressions for each of the terms making up V are derived in Budd *et al.* (2003). To extend this two-layer model to a multi-layer formulation we assume as before that there are $2n+1$ layers each of width Δt and length L and that $w_{i\Delta t}(x), i = -n \ldots n$ is the vertical deflection of the interface between two succesive layers. In the experiments conducted, each of the layers is compressed by the load by *the same horizontal amount* $\mathcal{E}$. The simplest way to ensure this occurs with the level set formulation is to set $\dot{w}(0) = \dot{w}(L) = 0$. The total energy of the multi-layer material can then be expressed as

$$U_B = \frac{Eb\Delta t^3}{24} \sum_{i=-n}^{n} \int_0^L \frac{\ddot{w}_i^2}{1-\dot{w}_i^2}\, \mathrm{d}\sigma, \tag{4.2}$$

$$U_F = \int_0^L [Q(w_n) - Q(w_{-n})]\, \mathrm{d}\sigma \tag{4.3}$$

$$P\mathcal{E} = P \int_0^L \left(1 - \sqrt{1-w_0^2}\right) \mathrm{d}\sigma \tag{4.4}$$

$$U_\mu = \mu R \Delta t \sum_{i=-n}^{n} \int_0^L \left|\sin^{-1}(\dot{w}_i)\right| \mathrm{d}\sigma. \tag{4.5}$$

where b is the breadth of the paper and dots denote differentiation with respect to σ. In this expression the external foundation is assumed to have a Winkler force law, so that the force resisting a *local* deflection w is given by $q(w) = dQ/dw$. We also assume that there is a *constant* reaction R between each of the layers and that the coefficient of friction μ between the layers is the same as that between the top and bottom layer and the external foundation. It is very important to observe that the bending energy has a component which varies as the integral of $\ddot{w}^2$. As we have already seen, this term becomes unbounded as we approach a singularity, and the expression (4.2) is not defined at this point. For the present we will assume that no singularity has formed so that this issue does not arise, and will return to consider the singular case. We can now combine the geometric description of the layers of with the mechanical description in the previous sub-section by expressing V in terms of the single function ϕ. Before we reformulate the energy contribution in terms of the level set fuction ϕ, it is useful to state a lemma that expresses various of the terms which arise in the energy expression in terms of ϕ

Lemma 4.1. *(a) The derivatives of x and y with respect to σ are as follows:*

$$\frac{\partial x}{\partial \sigma} = \dot{x} = \frac{\phi_y}{|\nabla \phi|}, \quad \frac{\partial y}{\partial \sigma} = \dot{y} = -\frac{\phi_x}{|\nabla \phi|} \tag{4.6}$$

(b) The curvature κ can be expressed as

$$\kappa = \nabla \cdot \frac{\nabla \phi}{|\nabla \phi|} = \frac{\phi_{xx}\phi_y^2 - 2\phi_y\phi_x\phi_{xy} + \phi_{yy}\phi_x^2}{\left(\phi_x^2 + \phi_y^2\right)^{\frac{3}{2}}} \tag{4.7}$$

(c) The angle of the tanjent θ is given by

$$\sin(\theta) = \frac{\partial w}{\partial \sigma} \quad \textit{and} \quad \kappa = \frac{\partial \theta}{\partial \sigma}. \tag{4.8}$$

Proof see Sethian (1999).

We now use these expressions to reformulate the various components of the energy contributions (4.2) and (4.5) in terms $\phi(x, y, t)$ where, to simplify the expression we set $\phi^i = \phi(x, y, i\Delta t)$ where $\phi^i(x, w_{i\Delta t}(x))$.

Theorem 4.2. *In the case of a* nonsingular *deformation the energy terms are given by*

$$U_B = \frac{Eb\Delta t^3}{24} \sum_{i=-n}^{n} \iint_\Omega \delta(\phi^i) \left(\nabla \cdot \frac{\nabla \phi^i}{|\nabla \phi^i|}\right)^2 |\nabla \phi^i| \, \mathrm{d}y \, \mathrm{d}x \tag{4.9}$$

$$U_F = \iint_\Omega \left[\delta(\phi^n)|\nabla \phi^n| Q(y_n) - \delta(\phi^{-n})|\nabla \phi^{-n}| Q(y_{-n})\right] \, \mathrm{d}y \, \mathrm{d}x \tag{4.10}$$

$$P\mathcal{E} = P \iint_\Omega \delta(\phi^0) \left(|\nabla \phi^0| + \phi_y^0\right) \, \mathrm{d}y \, \mathrm{d}x \tag{4.11}$$

$$U_\mu = \mu q \Delta t \sum_{i=-n}^{n} \iint_\Omega \delta(\phi^i) \left|\sin^{-1}\left(\frac{\phi_x^i}{|\nabla \phi^i|}\right)\right| |\nabla \phi_y^i| \, \mathrm{d}y \, \mathrm{d}x \tag{4.12}$$

The delta function is included in equations (4.9)-(4.12) so that it is the position of the *zero level set*, $\Gamma_{i\Delta t}$, that makes the contributions to the energy and not the part of ϕ defined over the rest of Ω. To determine V from this expression the delta function would have to be numerically approximated and this could potentially cause the evaluation of the integrals to be inaccurate. However, having located the zero level set of ϕ using the contour plotting algorithm and given the form of the function $\phi^i(x,y)$, a more direct approach can be used. To do this we formulate the equations over each zero level set, $\Gamma_{i\Delta t}$ to give the following result

Lemma 4.3 *Integrating over each level set we have*

$$U_B = \frac{Eb\Delta t^3}{24}\sum_{i=-n}^{n}\int_{\Gamma_{i\Delta t}}\left(\nabla\cdot\frac{\nabla\phi^i}{|\nabla\phi^i|}\right)^2\frac{|\nabla\phi^i|}{\phi^i_y}\,\mathrm{d}x \tag{4.13}$$

$$U_F = \int_{\Gamma_{n\Delta t}} Q(y_n)\frac{|\nabla\phi^n|}{\phi^n_y}\,\mathrm{d}x - \int_{\Gamma_{-n\Delta t}} Q(y_{-n})\frac{|\nabla\phi^{-n}|}{\phi^{-n}_y}\mathrm{d}x \tag{4.14}$$

$$P\mathcal{E} = P\int_{\Gamma_{i\Delta t}}\left(1+\left(\frac{\phi^0_y}{|\nabla\phi^0|}\right)\right)\frac{|\nabla\phi^0|}{\phi^0_y}\,\mathrm{d}x \tag{4.15}$$

$$U_\mu = \mu R\Delta t\sum_{i=-n}^{n}\int_{\Gamma_{i\Delta t}}\left|\sin^{-1}\left(\frac{\phi^i_x}{|\nabla\phi^i|}\right)\right|\frac{|\nabla\phi^i|}{\phi^i_y}\,\mathrm{d}x \tag{4.16}$$

Proof. We prove both the theorem and the lemma by considering each of the contributions to the energy in turn.

The bending energy The total bending energy of the multi-layer system is given by equation (4.2). Now, the curvature, κ, is defined as $\partial\theta/\partial\sigma$ and the tanjent angle by $\sin(\theta)=\dot{w}$. Hence

$$\kappa = \dot{\theta} = \frac{\mathrm{d}\theta}{\mathrm{d}\dot{w}}\frac{\mathrm{d}\dot{w}}{\mathrm{d}\sigma} = \frac{\mathrm{d}\theta}{\mathrm{d}\dot{w}}\ddot{w} = \frac{\ddot{w}}{\cos\theta} = \ddot{w}\left(1-\dot{w}^2\right)^{-\frac{1}{2}} \tag{4.17}$$

Therefore, if κ_i is the curvature on the curve $\Gamma_{i\Delta t}$ then the equation (4.2) can be written as

$$U_B = \frac{Eb\Delta t^3}{24}\sum_{i=-n}^{n}\int_0^L \kappa_i^2\,\mathrm{d}\sigma \tag{4.18}$$

Using the expression (4.7) it follows that the bending energy is given by

$$\begin{aligned} U_B &= \frac{Eb\Delta t^3}{24}\sum_{i=-n}^{n}\delta(\phi^i)\int_0^L\left(\nabla\cdot\frac{\nabla\phi^i}{|\nabla\phi^i|}\right)^2\mathrm{d}\sigma \\ &= \frac{Eb\Delta t^3}{24}\sum_{i=-n}^{n}\int_{\Gamma_{i\Delta t}}\left(\nabla\cdot\frac{\nabla\phi^i}{|\nabla\phi^i|}\right)^2\frac{|\nabla\phi^i|}{\phi^i_y}\,\mathrm{d}x \end{aligned}$$

The foundation energy By definition the vertical displacement w is the same as y such that $\phi(x,y,t)=0$. So that

$$\int_0^L\left[Q(w_{-n})-Q(w_n)\right]\mathrm{d}\sigma = \int_{\Gamma_{-n\Delta t}} Q(y_{-n})\frac{|\nabla\phi^{-n}|}{\phi^{-n}_y}\mathrm{d}x - \int_{\Gamma_{n\Delta t}} Q(y_n)\frac{|\nabla\phi^n|}{\phi^n_y}\,\mathrm{d}x. \tag{4.19}$$

The work done by the load We have assumed that each layer undergoes the same end-shortening under the axial load P and therefore the work done by the load is the same for one layer as for multiple layers. We arbitrarily choose to measure the end-shortening of the reference layer, $i = 0$.

$$\begin{aligned} P\mathcal{E} &= P\int_0^L \left(1-\sqrt{1-\dot{w}_0^2}\right)\,\mathrm{d}\sigma = P\int_0^L (1-x_\sigma^0)\,\mathrm{d}\sigma \\ &= P\int_0^L \left(1+\left(\frac{\phi_y^0}{|\nabla\phi^{\frac{n}{2}}|}\right)\right)\,\mathrm{d}\sigma = P\int_\Gamma \left(1+\left(\frac{\phi_y^0}{|\nabla\phi^{\frac{n}{2}}|}\right)\right)\frac{|\nabla\phi^0|}{\phi_y^0}\,\mathrm{d}x \end{aligned}$$

The work done against friction If we substitute (4.6) into (4.5) we obtain the expression

$$U_\mu = \mu q\Delta t\sum_{i=-n}^{n}\int_0^L \left|\sin^{-1}\left(-\frac{\phi_x^i}{|\nabla\phi^i|}\right)\right|\,\mathrm{d}\sigma = \mu q\Delta t\sum_{i=-n}^{n}\int_\Gamma \left|\sin^{-1}\left(\frac{\phi_x^i}{|\nabla\phi^i|}\right)\right|\frac{|\nabla\phi^i|}{\phi_y^i}\,\mathrm{d}x$$

□

(*b*) *The energy close to a singularity*

To refine this calculation we briefly consider the form taken by the bending energy close to a singularity where the curve Γ_t develops an infinite curvature when $t = T$. In this calculation we will assume that the reference layer Γ_0 is a smooth curve, with maximum curvature of $K > 0$ occuring at a minumum point where it has a locally parabolic form. As $t \to T = 1/K$ the maximum curvature of the curve Γ_t increases, and hence the bending energy also increases. To determine the asymptotic behaviour of the bending energy we will approximate Γ_0 locally by the parabola $y = Kx^2/2$, with $-1 < x < 1$. It then follows from the analysis presented in §2 that if $t = 1/K - \delta$ with $\delta > 0$ small, then the maximum curvature $\hat{\kappa_t}$ of the folded layer is given by $\hat{\kappa} = 1/\delta$. Similarly, if $t = 1/K$ then close to the point $x = 0$ the second derivative of the profile of the singular layer is given by $d^2y/dx^2 = K^{1/3}Ax^{-2/3}$, where $A = 2^{1/3}/3$. Note that $1/\delta = K^{1/3}Ax^{-2/3}$ if $x = L \equiv A^{3/2}K^{1/2}\delta^{3/2}$. The function d^2y/dx^2 obtained by a numerical differentiation of the Lagrangian formulation is illustrated in figure 13(a), where we take $K = 1$ and $\delta = 0.01$. In this figure we compare this second derivative both with the function $K^{1/3}Ax^{-2/3}$ and with the maximum estimate of K/δ.
For δ small, it is clear from this figure that we can estimate the function d^2y/dx^2 close to the point $x = 0$ by

$$d^2y/dx^2 \approx 1/\delta \quad \text{if} \quad |x| < L, \quad d^2y/dx^2 \approx K^{1/3}Ax^{-2/3} \quad \text{if} \quad |x| > L.$$

This estimate allows us to make an asymptotic estimate for the bending energy in terms of δ. As the dominant contribution to the bending energy occurs close to the singular region at $x = 0$ where dy/dx is small, we may closely approximate the curvature by the second derivative so that in the limit of $\delta \to 0$

$$\int \kappa^2 dx \int (d^2y/dx^2)^2 dx \approx 8KA^{3/2}\delta^{-1/2}.$$

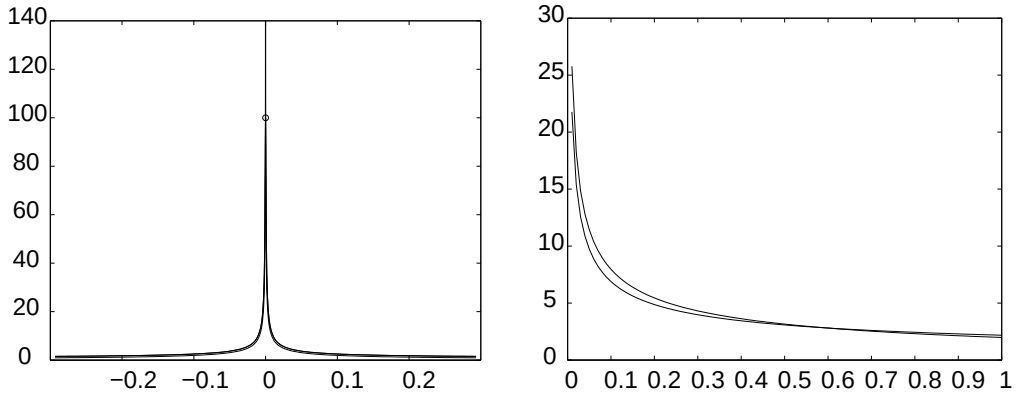

Figure 13. (a) The numerically computed curvature, compared with the asymptotic estimate of $K^{1/3}Ax^{-2/3}$ and the maximum estimate of $1/\delta$ (b) The numerically computed integral of $(d^2y/dx^2)^2$ plotted as a function of δ compared with the asymptotic estimate $8KA^{3/2}/\sqrt{\delta}$.

Hence we have the asymptotic estimate that as t approaches $1/K$ there is a constant B so that

$$u_B \sim B(1/K - t)^{-1/2}. \tag{4.20}$$

In figure 13(b) we compare a numerically computed integral of the bending energy with the asymptotic estimate and see good agreement.

(c) *Deformation profile for a particular of reference layer profile*

To determine the configuration of the multi-layer material we must determine the stationary values of the energy functional over all possible configurations of the reference layer Γ_0. This is difficult in general as Γ_0 can take many possible forms, leading to non-unique solutions. A study of some of these for a two-layer material, obtained by approximating Γ_0 by cubic-splines is described in Hunt *et al.* (2006). To make progress in the multi-layer problem, we will, for the present, restrict the class of solutions to those for which the reference deflection Γ_0 has a sinusoidal profile. Of course this is a restrictive class of solutions, but an inspection of figure 2 shows this to be not unreasonable for certain configurations. A fundamental difference between this calculation and earlier approaches is that we only make the assumption that the *reference* layer is a sinusoid, but allow other layers to take different profiles. In other calculations it has been assumed that *all* of the layers have a sinusoid form. This has led to significant underestimates of the total bending energy. Hence, for this calculation, we make the approximation (see Edmunds *et al.* (2006)) that Γ_0 is given in terms of the arc-length Σ by

$$\Gamma_0 = \{(x, y) : y = w_0(\sigma) = Q\cos\left(\frac{\pi\sigma}{L}\right)\}, \tag{4.21}$$

and proceed to calculate the other layer profiles using the LSM. For convenience we restrict the calculation to the half-wavelength of total arc-length L given by taking $0 \leq \sigma < L$. This profile has a local minimum with maximum curvature K given by $K = Q\pi^2/L^2$. We assume further that the value of L is known a-priori from the

linear buckling length-scale (Peletier 2001; Budd *et al.* 2003) and that the value of Q is to be determined. For a given value of Q the horizontal shortening of the layers is given

$$\mathcal{E} = L - \int_0^L \sqrt{1 - w_{0,\sigma}^2}\, \mathrm{d}\sigma. \tag{4.22}$$

To determine Q numerically we calculate the level set function ϕ, evaluate the bending energy using the formulae in lemma 4.3, and then find for which values of Q this is stationary. To calculate ϕ a computational grid is set up over a rectangle by dividing the horizontal region $[0, L - \mathcal{E}]$ into $M_1 - 1$ equal intervals of size h such that $x_j = jh, \quad j = 1, \cdots, M$. A similar division is made of the vertical region into M_2 regions of width h so that $y_k = kh$. The value of h is chosen to be consistent with the CFL condition, given that the time-step is determined by the layer thickness Δt. In practice it is often convenient to calculate the level sets at more refined intervals than the layers themselves, so we may take a time-step Δ for calculating ϕ given by $\Delta = \Delta t/m$ where m is a suitable integer. The level set problem is then initialized by taking

$$\phi_{kj}^0 = y_k - Q\cos\left(\frac{\pi\sigma_j}{L}\right) \quad \text{with} \quad x_j - \int_0^{\sigma_j} \sqrt{1 - w_{0,\sigma}^2}\, \mathrm{d}\sigma = 0 \tag{4.23}$$

The approximate values of ϕ are then determined at time intervals of Δ by using the methods outlined in §3 and the level sets Γ found by using the MATLAB `contour` function. The integrals (4.13)–(4.16) are evaluated using a 16 point Gaussian Quadrature rule at every m time steps (corresponding to each layer), and finally, the variation of the total energy V with respect to small changes in Q is found using central differences. The linear dependence of the total energy on the (fixed) load P allows us to find P as a function of the single variable Q without solving nonlinear equations. In particular, setting $\partial V/\partial Q = 0$ we have simply

$$P = \frac{\partial U_B/\partial Q + \partial U_F/\partial Q + \chi \partial U_\mu/\partial Q}{\partial \mathcal{E}/\partial Q}. \tag{4.24}$$

A plot of the resulting $(\mathcal{E}, P)$ curve in the case of a material with $n = 220$ layers of width 0.1mm and with $L = 35.9$mm is given in figure 14. Here we have taken $M = 180$ which corresponds to $h \approx 0.22$.

Using the previous theory we can understand the qualitative form of this figure. If Q is small then each of the terms $U_B, U_F, \mathcal{E}$ are locally quadratic functions of Q and hence their derivatives vary linearly with Q. However, U_μ is a locally linear function of Q and its derivative is linear. Thus as $Q \to 0$ the load P tends to ∞ (Budd *et al.* 2003). In contrast, as Q increases further, so the deflection of the layers furthest from the reference layer becomes more nearly singular. As the maximum curvature of the reference layer is given by $K = Q(\pi/L)^2$ and the half thickness t of the total layer is given by $t = n\Delta t$ it follows from the previous subsection, that the bending energy varies as

$$U_B \sim \frac{B}{\sqrt{L^2/(\pi^2 Q) - n\Delta t}}.$$

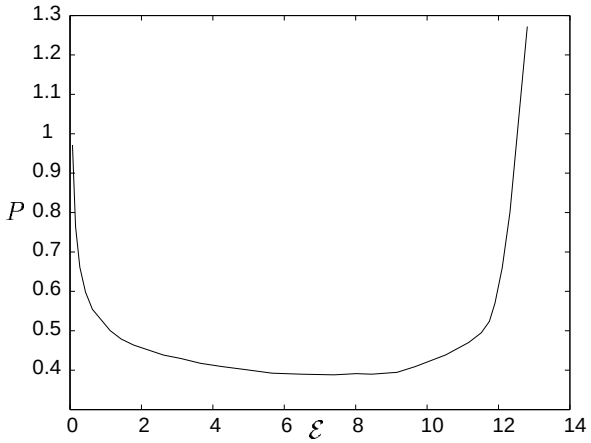

Figure 14. A plot of axial load against end shortening, showing that the bending energy re-stiffens the system

In particular, if $Q_S = L^2/\left(\pi^2 n \Delta t\right)$ the bending energy U_B becomes unbounded as $Q \to Q_S$ and there is a constant C so that $U_B \approx C/\sqrt{Q_S - Q}$. Hence, as the end-shortening only varies slowly with Q as $Q \to Q_S$ we conclude from (4.24) that as $Q \to Q_S$ we have $P \sim (Q_S - Q)^{-3/2}$. Mechanically, the formation of the singularity in the material is equivalent to a dramatic re-stiffening of the whole system, seen also in other folding configurations such as kink banding (Wadee *et a.* 2004). Of course we do not see an infinite load in practice, and for the rock formations considered in this paper we would expect to see some sort of fracturing or plastic behaviour in this limit, or alternatively the formation of multiple folds.

5. Conclusions

This paper has shown the potential of the level set method when modelling multi-layer problems. The ability to model parallel folding has been presented and it is anticipated that it can be adapted to model other folding scenarios. The level set method naturally encodes the nonlinear terms. The model is designed only to model the formation of the first hump. If extra humps are to be formed it will be important to understand what happens as the layers lockup, and the role that the singularities have in this (Hunt *et al.* 2006). It is interesting that the formation of singularities is purely due to the geometry and yet these singularities then impact on the system in a way which is presently unclear.

References

Budd, C. J., Edmunds, R. & Hunt, G. W. 2003 A nonlinear model for parallel folding with friction. *Proc. R. Soc. Lond. A* **459**, 2097–2119.

Chopp, D. L. 1993 Computing minimal surfaces via level set curvature flow. *J. Comp. Phys.* **142(2)**, 495–518.

Courant, R., Friedrichs, K. & Lewy, H. 1928 Über die partiellen differenzengleichungen der mathematischen physik. *Mathematische Annalen* **100(1)**, 32–74.

Crandall, M. G. & Lions, P. L. 1983 Viscosity solutions of Hamilton–Jacobi equations, *Tran. AMS* 277, 1–42.

Crandall, M. G., Evans, L. C. & Lions, P. L. 1984 Some properties of viscosity solutions of Hamilton–Jacobi equations. *Tran. AMS* **282**, 487–502.

Dervieux, A. & Thomasset, F. 1979 A finite element method for the simulation of Rayleigh–Taylor instability. *Lecture notes in mathematics* **771**, 145–159.

Dervieux, A. & Thomasset, F. 1981 Multifluid incompressible flows by a finite element method. *Lecture notes in Physics* **11**, 158–163.

Edmunds, R., Hunt, G. W. & Wadee, M. A. 2006 Parallel folding in multilayered structures. *J. Mech. Phys. Solids* **54**, 384–400.

Enright, D., Fedkiw, R., Ferziger, J. & Mitchell, I. 2002 A hybrid particle level set method for improved interface capturing. *J. Comp. Phys.* **183**, 83–116.

Enright, D. & Fedkiw, R. 2003 Robust treatment of interfacs for fluid flows and computer graphics. *HYP 2002* Eds. Hou, T & Tadmor, E. 153–164 New York: Springer-Verlag.

Hunt, G. W., Peletier, M. A. & Wadee, M. A. 2000 The Maxwell stability criterion in pseudo-energy models of kink banding. *J. Struct. Geol.* **22**, 669–681.

Hunt, G. W., Edmunds, R., Budd, C. J. & Cosgrove, J. W. 2006 Serial parallel folding with friction: a primative model using cubic B-splines. *J. Struct. Geol* **28**, 444–455.

Jiang, G.-S. & Peng, D. 2000 Weighted ENO schemes for Hamilton–Jacobi equations. *SIAM J. Sci. Comput.* **21**, 2126–2143.

Osher, S. & Fedkiw, R. 2003 *Level set methods and dynamic implicit surfaces.* New York: Springer-Verlag.

Osher, S. & Sethian, J. A. 1988 Fronts propagating with curvature-dependent speed: algorithms based on Hamilton–Jacobi formulations. *J. Comp. Phys.* **79**, 12–49.

Peletier, M. A. 2001 Generalised monotonicity from global minimization in fourth-order ordinary differentail equations. *Nonlinearity* **14(5)**, 1221–1238.

Price, N. J. & Cosgrove, J. W. 1990 *Analysis of geological structures.* Cambridge: Cambridge University Press.

Rhee, C., Talbot, L. & Sethian, J. A. 1995 Dynamical study of a premixed V flame. *J. Fluid Mech.* **300**, 87–115.

Russo, G. & Smereka, P. 2000 A level-set method for the evolution of faceted crystals. *SIAM J. Sci. Comput.* **21** 2073–2095.

Sethian, J. A. 1985 Curvature and the evolution of fronts. *Comm. in Math. Phys.* **101(4)**, 487–499.

Sethian, J. A. 1999 *Level set methods and fast marching methods: evolving interfaces in computational geometry, fluid mechanics, computer vision, and materials science.* Cambridge: Cambridge University Press.

Thompson, J. M. & Hunt, G. W. 1973 *A general theory of elastic stability.* Wiley.

Wadee, M. A., Hunt, G. W. & Peletier, M. A. 2004 Kink band instability in layered structures. *J. Mech. Phys. Solids* **52(5)**, 1071–1091.